Constraining optimum swimming strategies in plesiosaurs: The effect of amplitude ratio on tandem pitching foils

Cite as: Phys. Fluids **34**, 051908 (2022); https://doi.org/10.1063/5.0088453
Submitted: 17 February 2022 • Accepted: 28 April 2022 • Accepted Manuscript Online: 29 April 2022 • Published Online: 18 May 2022

Ali Pourfarzan and Jaime G. Wong

Physics of Fluids ARTICLE scitation.org/journal/phf

Constraining optimum swimming strategies in plesiosaurs: The effect of amplitude ratio on tandem pitching foils

Cite as: Phys. Fluids **34**, 051908 (2022); doi: 10.1063/5.0088453
Submitted: 17 February 2022 · Accepted: 28 April 2022 ·
Published Online: 18 May 2022

Ali Pourfarzan[a] and Jaime G. Wong

AFFILIATIONS

Department of Mechanical Engineering, University of Alberta, Edmonton, Alberta T6G 1H9, Canada

[a]Author to whom correspondence should be addressed: pourfarzan@ualberta.ca

ABSTRACT

Identical tandem flippers of plesiosaurs, which are unique among all animals, have been a source of debate regarding the role of hind flippers in their locomotion. Here, inspired by the kinematics of plesiosaur flippers, the effect of the amplitude ratio on the propulsive performance of in-line tandem pitching foils is investigated through a series of particle image velocimetry experiments. Three leader-to-follower amplitude ratios are considered for the foils pitching over a range of 0–2π phase difference. For the first time, it is shown that the amplitude ratio can significantly affect the performance of the hind foil at spacing larger than one chord length. It is found that the thrust generation of the hind foil at the optimum phase difference augments by 130% when it is pitching at the twice angular amplitude of the upstream foil. Although the total performance of the rear-biased and equal amplitude models reaches similar values, thrust production of the hind foil in the equal amplitude model increases only by 23%. By contrast, the performance of the forward-biased model decreases drastically for all phase differences due to the destructive wake–foil interaction of the hind foil. Studying the instantaneous wake–foil interactions, it is found that high thrust generation is associated with the formation of a vortex pair on the suction side of the hind foil, which causes stronger trailing edge vortices to shed with a greater total wake spacing. Finally, through scaling analysis, high-thrust configurations of tandem models are ranked based on the total efficiency of the system.

I. INTRODUCTION

Plesiosaurs, Mesozoic marine reptiles, are known for their body planform, unique among all extinct and existing animals. They exhibit identical wing-like tandem flippers, leading to controversial discussions on their locomotion, and in particular, regarding the role of the hind flipper in propulsion, known as the "four-wing" problem.[1] Throughout the evolution of plesiosaurs, the similarity in the size and geometry between the fore and hind flippers of the reptiles remained consistent. This is indicative of a high importance of this characteristic for plesiosaurs fitness. It was suggested that plesiosaurs with long necks and small heads were ambush predators, whereas plesiosaurs with short necks and large heads, also known as pliosaurs, were pursuit predators.[2,3] Generally, natural swimmers and flyers are capable of both impressive acceleration and maneuvering, and highly efficient cruising. These traits have led to significant interest in biological swimming and flight in the context of biomimetic and bio-inspired aero- and hydrodynamics. Many animals propel themselves by flapping their wings, flippers, or tail fins. Biologically inspired flapping propulsion is often abstracted by oscillating foils.[4,5] A wide range of experiments and numerical simulations have been carried out to reveal the flow dynamics and other aspects associated with the performance of oscillating foils, for instance as reviewed by Wu *et al.*[6]

An early investigation of thrust generation by a flapping airfoil was provided by Knoller and Verein[7] and Betz[8] independently. It was discovered that the oscillatory nature of flapping motion leads to oscillatory lift, and subsequently the generation of force in the direction of flight, a phenomenon known as the Knoller–Betz effect.[9] The motion of an oscillating foil can be characterized with the Strouhal number, defined as $St = 2Af/U_\infty$, where A denotes amplitude, f is frequency, and U_∞ is the freestream velocity. The Strouhal number is closely associated with force generation (e.g., see Baik *et al.*[10]) and may be conceptualized as the ratio of length scales of oscillation to convection. At low Strouhal numbers, a drag producing vortex street known as the Bénard–von Kármán wake forms in the wake of an oscillating foil. With increasing the Strouhal number, the vortex street eventually inverts to become a so-called reverse Bénard–von Kármán wake,[11]

which roughly coincides with the transition from a drag producing to a thrust producing wake.[12,13] This flow pattern is very similar to that formed in the wake of natural flapping propulsors, subject to minor differences associated with flapping (rotation about a shoulder joint) vs quasi-2D oscillation.[14,15] Natural flyers and swimmers have been observed to flap their wings and flippers within a only a narrow range, $0.2 < St < 0.4$ in cruising conditions across a wide range of Reynolds numbers and biological origination.[16,17] This range coincides with the optimal propulsive efficiency observed in oscillating foil experiments.[4,18] Experiments by Jones *et al.*[19] demonstrated that the transition from thrust generation to drag production occurs in the wake of an oscillating foil when the amplitude of oscillation was increased beyond a certain critical point for fixed Strouhal number. Meanwhile, a closely related similarity parameter is the reduced frequency, $k = \pi fc/U_\infty$,[20] which can be interpreted as the ratio of the timescale of oscillation to the timescale of freestream convection, characterizing the degree of unsteadiness imposed by oscillation in the flow. Here, c denotes the chord length of the oscillating foil. Numerous studies have shown that while thrust increases with reduced frequency, high efficiencies are achieved at relatively low reduced frequencies.[6]

For many flyers and swimmers in nature, locomotion is achieved through the interaction of multiple propulsors. For example, many fish generate thrust via complex interactions between the caudal fin and the vortices shed in the wake of the dorsal fin positioned upstream.[15,21] Similarly, dragonflies adjust the phase between the fore and hind wings to switch between different flight modes.[22] Akhtar *et al.*[23] modeled the dorsal and tail fin interaction of bluegill sunfish via in-line pitching and heaving tandem foils. They showed that at the correct phase difference (ϕ) between the foils, the vortices shed from the upstream foil causes the leading edge vortex (LEV) on the downstream foil to stall, which in turn increases the thrust and efficiency of the downstream foil significantly. Similar wake interactions were observed by Rival *et al.*[24] and Broering *et al.*,[25] where, inspired by dragonfly flight, they studied the effect of the phase difference between two tandem foils. Through the experiments[24] and numerical simulations,[24,25] they identified two distinct modes of either instantaneous high thrust generation, or energy extraction, depending on the phase difference. In each of the aforementioned studies, the spacing between the foils was kept constant within each study.

Other examples of tandem foil propulsion in nature include fish schooling[26–29] and bird flocking,[30,31] where favorable interactions within the flow allow neighboring animals to enhance the propulsive performance and efficiency by adjusting their flapping behavior (synchronization) and distance from the neighbor. Studies on tandem pitching foils[32,33] and tandem pitching and heaving foils[34–38] have shown that the propulsive performance of the downstream foil is primarily determined by the phase difference and spacing of the foils. For either case, the parameters adjust the time-of-arrival of the vortices shed from the upstream foil arriving at the downstream foil. Boschitsch *et al.*[32] investigated the full phase space range of $0 < \phi < 2\pi$ of tandem pitching foils across spacings of 0.25–4.25c, subject to high reduced frequencies and low amplitudes. In this configuration, it was demonstrated that, at spacings larger than 0.5c, the performance of the upstream foil was not affected by the presence of downstream foil, which was later confirmed by other studies.[35,36] They argued that the velocity induced by vortices shed from the upstream foil could result in leading edge separation on the downstream foil, and if this separation occurred on the suction side of that foil, as determined by the time-of-arrival, the resulting induced vortex increased lift and thrust generation by further dropping the pressure. This subsequently results in a wake mode characterized by high momentum and coherence.[32] Broader parametric studies have been conducted to address more complex tandem foil interactions, to better match behavior observed in nature. Joshi and Mysa[37] studied the effect of leader-to-follower chord ratio in the range of 0.25–1.0 for combined pitching and heaving of tandem foils across spacings of 1–10c at $k = 0.62$. They reported that maximum thrust decreases at smaller chord ratios due to the reduced energy in the wake of upstream foil. However, it was observed that efficiency remains larger at all chord ratios for high values of thrust. Kurt *et al.*[39] investigated the effect of follower-to-leader amplitude ratio across the range of 1–1.48 for phase difference of $0 < \phi < 2\pi$ at a fixed 0.5c spacing. They reported that the peak collective efficiency increases by 29%, where the collective thrust was enhanced by 63%–84%.

In the paleontology literature, it has been generally argued that plesiosaurs flapped their flippers dorso-ventrally to propel themselves, known as underwater flight or lift-based propulsion, similar to penguins and sea turtles.[2,40,41] Therefore, plesiosaur locomotion can be abstracted by tandem oscillating foils, which is a general wake–foil interaction and vortex dynamics problem. Liu *et al.*,[42] using inviscid flow simulations, studied the locomotion of plesiosaurs. Although they studied acceleration from rest, they concluded that plesiosaurs were reliant on the fore flippers for propulsion. More recently, Muscutt *et al.*,[41] using reconstructed plesiosaur flippers, experimentally showed that in cruising conditions, the hind flipper would have reached 60% higher thrust and 40% higher efficiency if both the fore and hind flippers flapped in harmony with a particular ideal phase difference. It was argued that the general flow and vortex shedding are independent of the flipper planform, as they are also observed in two-dimensional tandem flipper simulations. In their experiments, they considered the effect of spacing (either three or seven chord lengths) and the effect of frequency (Strouhal number) on the propulsive performance of the hind foil. However, both the fore and hind foils had the identical frequency and amplitude of oscillation in each of the configurations they investigated.

Although the physical planform of plesiosaur flippers was likely identical, the morphologies of the fore and hind flippers were slightly different. Fossil records show that the fore flippers of long-necked plesiosaurs had higher angular amplitude range than hind flippers,[42,43] and the pectoral (shoulder) girdles were more developed than pelvic girdles, unlike short-necked plesiosaurs (pliosaurs), which had more developed pelvic girdles.[44,45] Furthermore, assuming identical kinematics for both flippers is an ideal condition, which might not be the choice of an animal in the nature for cruising condition. In this study, inspired by the difference observed in morphologies and the angular excursion range between the plesiosaur's two sets of flippers, through a set of particle image velocimetry (PIV) experiments, we attempt to understand the effect of amplitude ratio on the propulsive performance of high-amplitude tandem pitching foils, and its relationship with the phase difference between the foils. Furthermore, we elaborate on the underlying mechanism of thrust generation in the studied configurations by analyzing the wake–foil interactions in detail. The results presented in the current work may be valuable to inform future

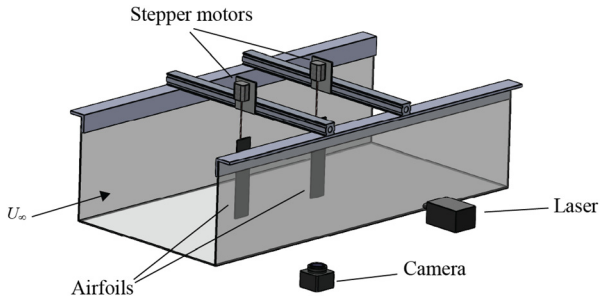

FIG. 1. Experimental setup and PIV configuration utilized in this study. The camera captured the flow field from the underneath of the water channel, while the laser illuminated the flow field from side.

studies focusing on plesiosaur locomotion or efficient marine/aerial vehicle design.

II. METHODOLOGY

The experiments were conducted in a recirculating open-surface water channel with a cross-section of 0.68×0.47 m, length of 5.2 m, and turbulence intensity of 4%.[46] The water depth was maintained at 0.35 m throughout the experiments. Two identical airfoils with a National Advisory Committee for Aeronautics (NACA) 0012 cross-section and $c = 0.069$ m chord were mounted vertically from above the channel (see Fig. 1). The airfoils were manufactured as continuous aluminum extrusions. To limit three-dimensional effects, the gap between the foils and the floor of the water channel were maintained at 5% of chord length. The pitching axis was the aerodynamic center of either airfoil and was driven by independent stepper motors (PK258-02Dl, Oriental Motor). Motion control was achieved by microcontroller. The fore foil was pitched harmonically at $\alpha_f = \alpha_{0,f} \sin(2\pi ft)$, while the hind foil was pitched with a phase difference (ϕ) at $\alpha_h = \alpha_{0,h} \sin(2\pi ft + \phi)$, where f is frequency, t is time, and $\alpha_{0,f}$ and $\alpha_{0,h}$ are the maximum angle of attack of the fore and hind foils, respectively.

In this study, the amplitude ratio is defined as the ratio of the maximum angles of attack of the fore foil to the hind foil (pitch amplitudes), $Ar = \alpha_{0,f}/\alpha_{0,h}$. This definition is slightly different than that given by Kurt *et al.*[39] describing the amplitude ratio as the ratio of trailing edge amplitudes of the foils. However, the difference in the numerical values of Ar determined by either derivation is small for the parameters in this study and therefore does not affect the results or the conclusion of this study. The trailing edge amplitude of the motion is obtained as $A_f = (3c/4)\sin(\alpha_{0,f})$ for the fore foil and $A_h = (3c/4)\sin(\alpha_{0,h})$ for the hind foil (Fig. 2). For all measurements, in order to isolate the effect of amplitude ratio (Ar) on the propulsive performance of the tandem system, all parameters except the amplitude of the fore foil (A_f) and phase difference (ϕ) between the foils, are constants. Three amplitude ratios of $Ar = 0.5$, 1.0, and 1.5 (represented, respectively, as $Ar_{0.5}$, Ar_1 and $Ar_{1.5}$ models) were investigated in this study. For each of the tandem models, 8 phase differences ($0 < \phi < 2\pi$ with $\pi/4$ increment) were set between the foils, totaling in 24 tandem pitching configurations to study. The free stream velocity was maintained at $U_\infty = 0.078$ m/s. The frequency of oscillation was identical for both foils at $f = 0.44$ s^{-1} throughout the experiments. Therefore, the chord-based Reynolds number was $Re_c = U_\infty c/\nu = 5382$ and the reduced frequency was $k = \pi fc/U_\infty = 1.22$, where ν is the kinematic viscosity of the water. The Reynolds number is within the range used in previous studies of tandem pitching foils.[32,33] The Strouhal number is defined based on the trailing edge amplitude of the foils as $St = 2Af/U_\infty$. As this study is inspired by plesiosaurs, the inter-foil spacing was set to $S = 3c$ to be consistent with the measurements of a recently studied specimen by Muscutt *et al.*[41] The pitching angle of the hind foils and fore foil of Ar_1 model was chosen as an average value of the dorso-ventral flapping angle of three plesiosaur specimens (67°) as reported by Muscutt,[47] and the pitch amplitude of the fore foils of $Ar_{0.5}$ and $Ar_{1.5}$ was chosen to closely represent the minimum and maximum flapping ranges measured from plesiosaur fossils, respectively.[42,47] Other parameters such as freestream velocity and frequency were picked to overlap the Strouhal number range observed in nature for efficient cruising conditions, that is, $0.2 < St < 0.4$.[16,17] A summary of the configurations and associated kinematics is presented in Table I. Although the effect of amplitude ratio is studied here with a coarse granularity, it should be noted that further decreasing the amplitude of the fore foil in order to study the effect of lower amplitude ratios would likely result in drag production by the fore foil, and such an investigation is beyond the scope of the present study.

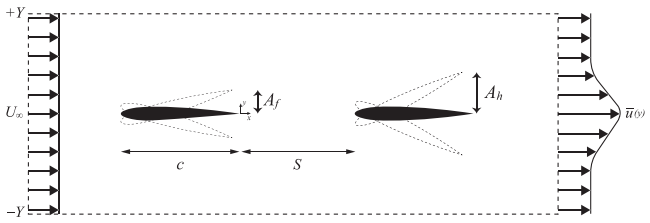

FIG. 2. Control volume surrounding the tandem foils.

The flow field was characterized with a PIV system composed of a Photron FASTCAM Mini WX50 high-speed camera (2048×2048 pixel^2 resolution, 10 μm pixel size), and a 5W continuous-wave Nd:YAG laser ($\lambda = 532$ nm). The high-speed camera was equipped with Nikon AF NIKKOR 20 mm f/2.8D lens. The flow was seeded with polymer microspheres with the diameter of 20 μm. The images were captured at 125 frames per second (fps) for single foils (fore foils) and 200 fps for hind foils. The shutter speed was set at 1/300 s during both single foil and hind foil recordings. PIV images were processed with in a commercial software package (LaVision DaVis 8.4.0). The final interrogation window with the size of 48×48 pixels and 50% overlap was selected to perform the vector calculations. Each of the test cases was repeated and recorded 10 times, and the results were ensemble-averaged in order to obtain the final vector fields.

TABLE I. Summary of the kinematics of fore and hind foils in each of the tandem configurations.

Model	Ar	$\alpha_{max,f(deg)}$	$\alpha_{max,h(deg)}$	St_f	St_h
$Ar_{0.5}$	0.5	16.5	33.5	0.17	0.32
Ar_1	1.0	33.5	33.5	0.32	0.32
$Ar_{1.5}$	1.5	50	33.5	0.45	0.32

Uncertainty of displacement in PIV measurements, which is suggested by Raffel *et al.*[48] to be 0.1 pixel as sub-pixel accuracy of particle locations, corresponds to 2% and 3.2% of free stream velocity in single foil and tandem foil measurements, respectively.

Mean thrust force on the airfoils was obtained by applying the integral momentum theorem to the control volume around the airfoils as shown in Fig. 2. As the variation of velocity with respect to time was sinusoidal for every oscillation cycle, it can be inferred that the unsteady momentum term should be zero when cycle-averaged. Therefore, the spatial integral of the cycle-averaged momentum flux was equivalent to the cycle-averaged of the spatial integral. Hence, the steady mean thrust coefficient was estimated via following equation:

$$\overline{C_T} = \frac{2}{c}\int_{-Y}^{+Y} \frac{\bar{u}(y)}{U_\infty}\left(\frac{\bar{u}(y)}{U_\infty} - 1\right) dy. \tag{1}$$

Here, the overbar in $\bar{u}(y)$ denotes the cycle-averaged streamwise velocity, which was performed over two cycles. The downstream control surface was $0.7c$ downstream of the trailing edge of the single foil or hind foil, respectively. In previous studies, it is well documented that the propulsive performance of the fore foil is not affected by the presence of hind foil when the inter-foil spacing is larger than one chord length ($S > 1c$).[32,35,36] Since the inter-foil spacing in all experiments in the present study was set to $S = 3c$, the thrust coefficient of isolated foils obtained here can be considered as the propulsive performance of the fore foils in tandem configurations ($Ar_{0.5}$, Ar_1, and $Ar_{1.5}$), if we wish to decompose the contributions to thrust.

III. RESULTS AND DISCUSSION

In this section, we first study the propulsive performance and the flow field of single isolated foils, with amplitudes matching forward foils of the three cases above. Then, we analyze the effect of amplitude ratio on the performance of tandem systems in terms of the flow field, wake–foil interactions, and the interactions of the wake structures of the high-performance and low-performance cases in all tandem models.

A. Propulsive performance of single foils

In order to provide a baseline for comparison, we obtained the time-averaged thrust of individual foils, with pitching kinematics matching the three different kinematic cases that would be used in tandem-foil tests later. The propulsive performance of single foil measurements obtained from the wake at $x/c = 0.7$ from the trailing edge is as follows: $\bar{C}_{T,f,0.5} = 0.02$, $\bar{C}_{T,f,1} = 0.13$, and $\bar{C}_{T,f,1.5} = 0.54$. As it is stated in Sec. II, these values are also representative thrust coefficients of fore foils in corresponding tandem configurations. Therefore, the results are denoted with additional subscripts corresponding to the analogous tandem-foil kinematics, to be consistent with Secs. III and IV It can be seen that the time-averaged thrust increases by increasing the Strouhal number, which is consistent with the literature.[32,33,49]

Comparing the performance of the single foils in this study to the ones obtained by Boschitsch *et al.*,[32] it can be seen that isolated foils in this study produce marginally less thrust at the same Strouhal number. This was expected and can be explained by considering the additional effect of the reduced frequency on the performance of a pitching foil. The foils in the present study are pitching at relatively high amplitudes and low reduced frequency than the ones studied by Boschitsch *et al.*[32] As shown by Jones *et al.*,[19] for a fixed Strouhal number, the propulsive performance of an oscillating foil decreases when the oscillation amplitude is increased beyond a certain limit.

The performance of the fore (single) foil of Ar_1, $\bar{C}_{T,f,1}$, will be used as reference to normalize the total performance obtained for the tandem systems. We chose it as reference case because the hind foil in all tandem configurations was pitching with the kinematics of the fore (single) foil of Ar_1 configuration. Hereafter, any data referred to as "reference" will refer to an isolated foil of this amplitude. This also corresponds to the average excursion amplitude of plesiosaur flippers (67°) as discussed in Sec. II. Therefore, the normalized performance of any tandem configuration exceeding $\bar{C}_T^* > 1$ is an indication of thrust augmentation if the hind flipper was involved in plesiosaur locomotion. Values exceeding $\bar{C}_T^* > 2$ in tandem configurations would demonstrate that tandem flippers as a system exceed the sum of its individual flippers in isolated (uncoupled) conditions and equivalent kinematics. Further analyses are provided in Sec. III C.

B. Flow field of single foils

The instantaneous normalized vorticity field and cycle-averaged velocity field over two cycles of the single foil are shown in Fig. 3. The instantaneous vorticity fields of isolated foils representing the corresponding fore foils of Ar_1 [Fig. 3(c) Multimedia view] and $Ar_{1.5}$ [Fig. 3(e)] show that a reverse Bénard–von Kármán vortex street is formed where two vortices of opposite sign shed per cycle, as expected. In the case of fore foil of $Ar_{0.5}$ [Fig. 3(a)] two like-signed vortices are observed to shed during each stroke. Note that the shadow cast by the foil and the regions obstructed by the parallax effect from the tip of the foil are covered with white polygon with gray edges. In these figures, vorticity is normalized as $\omega^* = \omega c/U_\infty$.

The vortices in the wake of the fore foil in $Ar_{1.5}$ are larger and stronger than Ar_1. In Fig. 3(c) (Multimedia view), focusing on the middle of the upstroke of the reference case, the leading edge vortex (LEV) forms on the lower surface of the foil during the upstroke (LEV-u) and rolls toward the trailing edge during the downstroke. Here "u" denotes upstroke. Once the LEV-u reaches the trailing edge at the end of the stroke, its strength decreases as it detaches and mixes with opposite-sign vorticity as the foils begins the next stoke. The weak LEV-u, after shedding, interacts with the TEV shed during the upstroke (TEV-u) and is partially annihilated. A similar interaction is seen for vortices of the single foil of $Ar_{1.5}$, except that in this case, the LEV-u detaches during the upstroke due to the very high pitching amplitude, yet remains close to the bottom surface until it reaches the trailing edge at the end of the downstroke. The time-averaged velocity fields of both fore foils of Ar_1 and $Ar_{1.5}$ [Figs. 3(d) and 3(f)] illustrate a jet wake behind the foils where the momentum of the jet is higher in $Ar_{1.5}$, consistent with the presence of stronger vortices observed in its wake. The cycle-averaged (two cycles) flow field figures are mirrored with respect to the center of the wake to remove the shadow cast by the foil in the laser sheet. In $Ar_{0.5}$ configuration [Fig. 3(a)], due to its low amplitude and low reduced frequency, it can be seen that circulation from the shear layer is shed as several smaller vortices, and the two like-signed primary vortices (TEV-u1 and TEV-u2) retain their coherence as they advect downstream. The time-averaged flow field of the single foil in $Ar_{0.5}$ in Fig. 3(b) demonstrates a weak jet in the middle of the wake, which corresponds to the small amount of thrust produced relative to the other isolated foils.

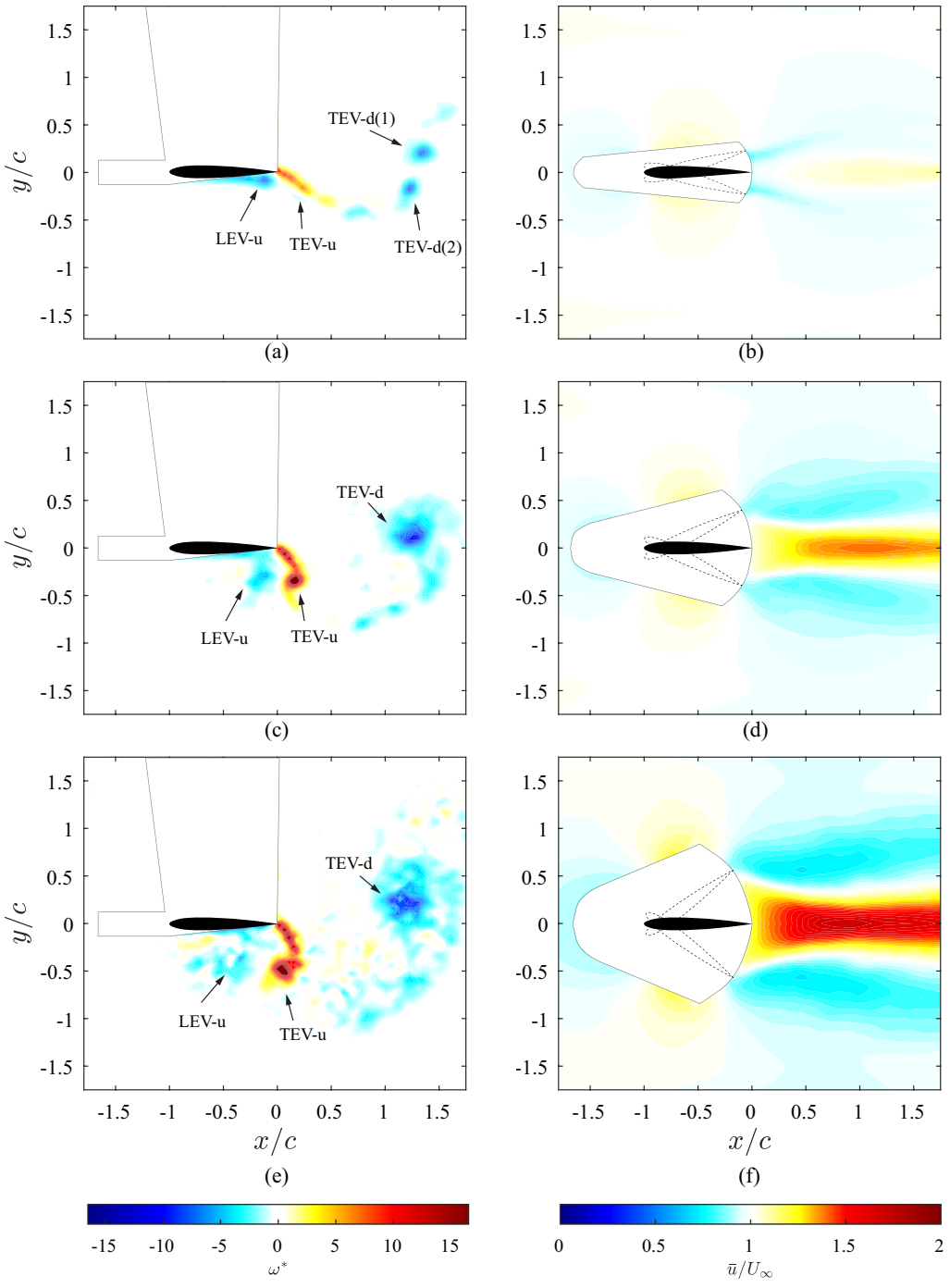

FIG. 3. Vorticity fields (left column) and cycle-averaged velocity fields (right column) of single foils representing fore foils of: (a) and (b) $Ar_{0.5}$, (c) and (d) Ar_1, and (e) and (f) $Ar_{1.5}$. Flow fields of (c) and (d) also represent the flow fields of reference single foil. Multimedia view of Fig. 3(c): https://doi.org/10.1063/5.0088453.1

C. Propulsive performance of tandem foils

Time-averaged thrust coefficients obtained for each of the models are presented in Fig. 4. These thrust coefficients represent the combined tandem foil system. Thrust coefficients presented in this figure are normalized with the value obtained for the reference single foil, that is, $\bar{C}_{T,f,1} = 0.13$. It should be noted, however, that the particular choice of normalization value does not affect the conclusions, as the relative performance of each case will remain the same. It can be seen

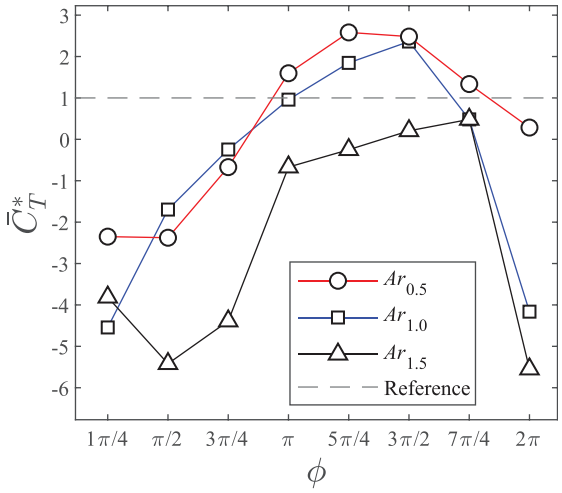

FIG. 4. Variation of time-averaged normalized thrust coefficients of tandem configurations, $\bar{C}_T^*$, with phase difference (ϕ) between the fore and hind foils, obtained at $x/c = 0.7$ from the trailing edge of the hind foil. The dashed line indicates the normalized performance of the reference single foil.

that the time-averaged thrust obtained for a tandem configuration is highest for the $Ar_{0.5}$ at $\phi = 5\pi/4$. For this case, the total thrust obtained is about 2.5 times of the value obtained for the reference flapping foil, meaning the hind foil approximately achieved 130% increase in thrust than it would have in isolation. This is to say that for this particular phase difference, the small addition to the wake momentum generated by the low-amplitude fore foil more than doubles the thrust produced by the hind foil. Generally, it is evident that $Ar_{0.5}$ configurations produce higher thrust (or lower drag, depending on the phase difference) compared to Ar_1 and $Ar_{1.5}$ configurations. This increase in performance can be explained with reference to the instantaneous flow field, which is the topic of Sec. III D.

The highest thrust producing configuration of $Ar_{0.5}$ ($\phi = 5\pi/4$) outperformed the highest-thrust case of Ar_1 ($\phi = 3\pi/2$), but only by approximately 10%. For this phase difference, Ar_1 produced 2.2 times the thrust of the reference case, such that the thrust produced by the hind foil in this configuration was only slightly augmented (23%) by the addition of the upstream foil. This relatively small increment was expected. In addition to the effect of lower reduced frequency in our experiments, as it has been shown by Boschitsch *et al.*,[32] the peak thrust and efficiency are achieved at spacings $S < 2.5c$ for in-line tandem pitching foils. Our results show that $Ar_{1.5}$, when the fore foil has higher amplitude than the hind foil, produced 56% less thrust than the reference case, even at its optimum phase difference ($\phi = 7\pi/4$). All other configurations of $Ar_{1.5}$ produced either negligible thrust or drag. Presented values of thrust coefficient in Fig. 4 are found to be completely periodic for $Ar_{0.5}$ and Ar_1 models. Additionally, it can be seen that the optimum phase difference between the fore and hind foils increases for increasing amplitude ratio. This increment is even more evident when we compare the optimum phase difference of $Ar_{0.5}$ at $\phi = 5\pi/4$ and $Ar_{1.5}$ at $\phi = 7\pi/4$.

From the paleontological perspective, as the $Ar_{0.5}$ model, representing a rear-biased locomotion, demonstrates superiority over other tandem models, it can be speculated that plesiosaurs could likely achieve higher performance by utilizing this type of locomotion. This swimming behavior is consistent with fossil records of short-necked plesiosaurs (pliosaurs), which exhibit more developed pelvic girdles than pectoral girdles. Meanwhile, fossil records of long-necked plesiosaurs exhibit relatively larger pectoral girdles, which is more consistent with forward-biased locomotion. However, as none of the configurations of $Ar_{1.5}$ model exceed the reference single foil performance, it is unlikely that they used this configuration for cruising locomotion. Another practicable model investigated in this study is Ar_1, which represents the equal-amplitude motion. Our results suggest that plesiosaurs could likely experience augmented performance by utilizing this type of locomotion, confirming the findings of Muscutt *et al.*[41] However, at the optimum phase difference, the hind foil in highest thrust phase of $Ar_{0.5}$ model achieves higher thrust than the one observed for Ar_1.

D. Flow field of tandem foils

In order to understand the mechanisms causing the various amplitude ratios to produce such high and low performances, we must investigate the instantaneous dynamics of the wake structures. Following this, we present a comparative analysis between the high-thrust cases of $Ar_{0.5}$ and Ar_1 configurations to further reveal the effect of amplitude ratio on the performance of an in-line tandem pitching system.

Model $Ar_{0.5}$: In the highest thrust case, corresponding to a phase difference between the foils of $\phi = 5\pi/4$, it is seen that the two small vortices shed from the fore foil (which is pitching at half amplitude of the hind foil), denoted by TEV-uf(1) and TEV-uf(2) in Fig. 5(a) (Multimedia view), arrive at the vicinity of hind foil at $t/T = 0.37$ at the beginning of the upstroke. Note that t/T in Fig. 5 refer to time within an oscillation cycle of the fore foil and not a phase difference. Hereafter, "f" and "h" are used in association with "LEV" and "TEV" to distinguish weather the vortex is shed from the fore ("f") or hind ("h") foil. The TEV-uf(2) is weaker than TEV-uf(1) and passes far above the surface of the foil and annihilates further at the downstream not affecting the performance. The TEV-uf(1), however, arrives at the leading edge at the middle of the upstroke $t/T = 0.62$ [Fig. 5(b), Multimedia view]. This instance is concurrent with the onset of formation of LEV-uh with the opposite sign. Since TEV-uf(1) has come very close to the leading edge, it induces the leading edge. As the upstroke proceeds, the TEV-uf(1) leaves the induced LEV-uh and quickly moves toward the trailing edge while remaining attached to the lower surface of the foil due to the suction. At the end of the upstroke at $t/T = 0.87$ [Fig. 5(c), Multimedia view], the TEV-uf(1) reaches to the trailing edge inducing a larger TEV-dh, which is going to be shed the next stroke, that is, downstroke. The TEV-uf(1) and the induced TEV-dh form a vortex pair which its (u_y) component of induced velocity causes the TEV-dh to shed at a farther lateral distance from the center of the wake compared to the TEVs shed from the reference foil. The TEV-dh shed from the lower surface of the foil induces the shear layer on lower surface which by the beginning of the downstroke will shed and amalgamate into the induced TEV-dh resulting in a stronger TEV than the one shed from the reference foil. This is confirmed as shown in Fig. 6 demonstrating the time history of the circulation evolution of the TEVs. The circulation of the vortices is calculated along the closed contour, which surrounds the vorticity. Values above 10% of the maximum vorticity were chosen to calculate the circulation. The vortex

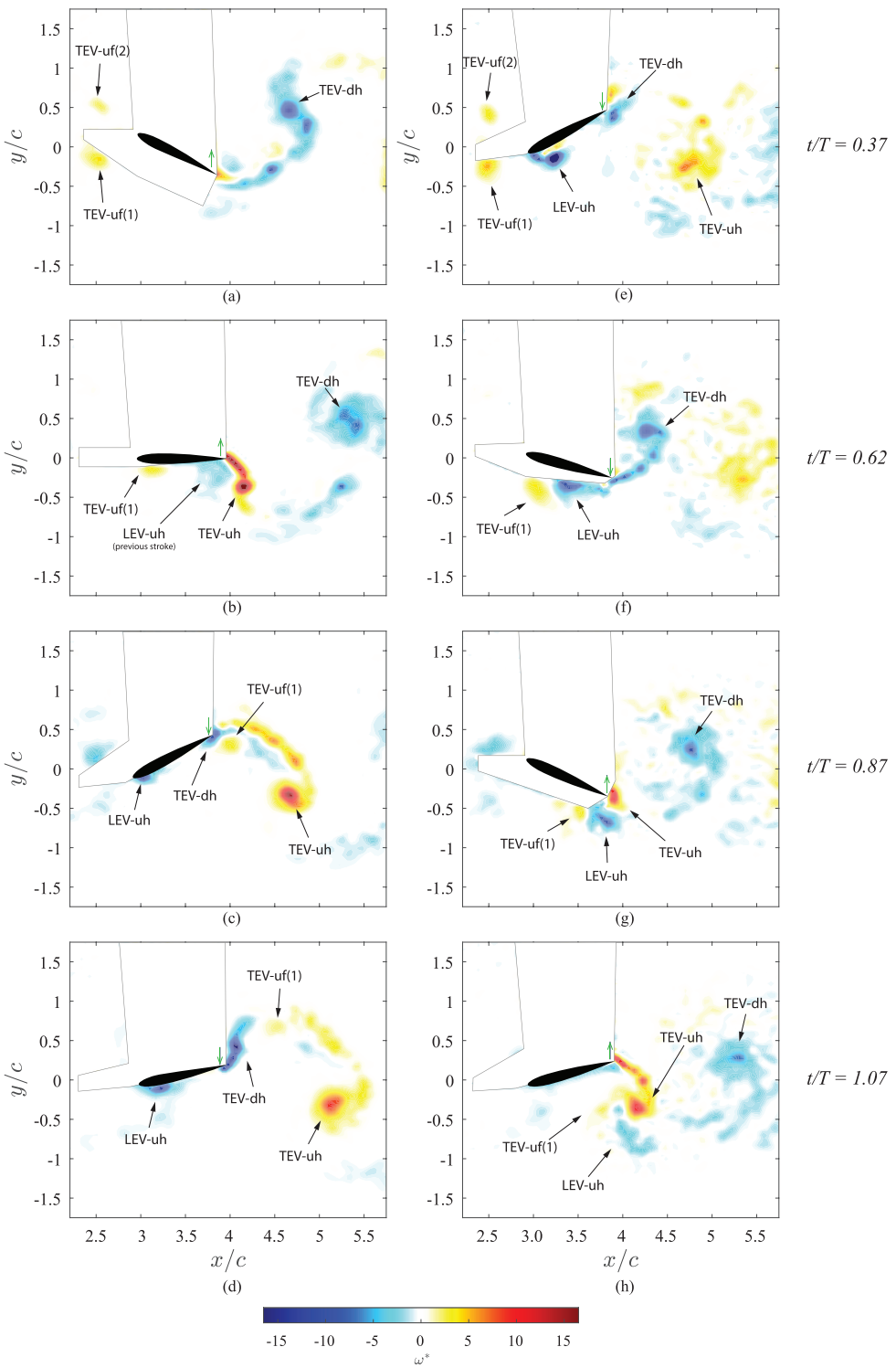

FIG. 5. Instantaneous vorticity fields of hind foil in model $Ar_{0.5}$ at: (a)–(d) $\phi = 5\pi/4$ corresponding to high-performance case and (e)–(h) $\phi = \pi/2$ corresponding to low-performance case. t/T denotes the time in the oscillation period of the fore foil. This figure illustrates the arrival of TEV-uf(1) at the hind foil and their interactions during one oscillation cycle of the hind foil. The green arrow positioned on the trailing edge demonstrates the instantaneous direction of the foil motion. Multimedia view of Figs. 5(a)–5(d): https://doi.org/10.1063/5.0088453.2

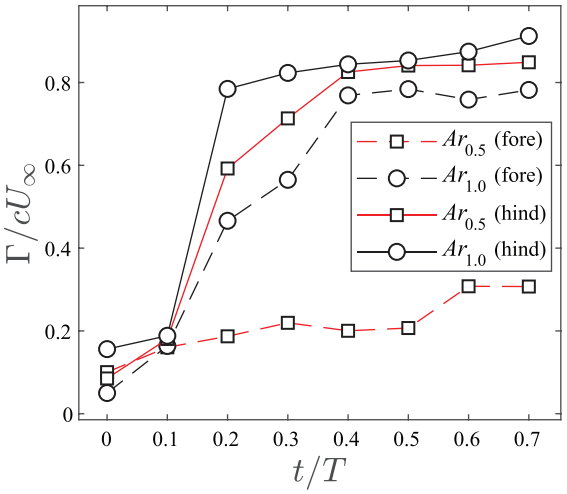

FIG. 6. Time-history evolution of circulation of TEVs shed from the pitching foil. $Ar_{0.5}$ (fore) data represent the circulation values of TEV-df(1) in Fig. 3(a), and Ar_1 (hind) represents the circulation values of TEV-df + LEV-uh in Figs. 8(b)–8(d). Note that Ar_1 (fore) data also represent the data of the reference single foil [TEV-u in Fig. 3(c)].

pair starts decoupling at the instance of TEV shedding and the onset of downstroke. At this instance, the vortex pair decouples constructively (without generating secondary wake structures), and while the TEV-dh continues growing because of the vorticity supply from the lower surface of the foil, the TEV-uf(1) joins the like-signed secondary structures from the vorticity tail of the TEV-uh shed from previous stroke. This becomes clearer later at $t/T = 1.07$ as the downstroke proceeds [Fig. 5(d), Multimedia view]. The LEV-uf formed at the middle of the upstroke eventually starts rolling down at the beginning of the downstroke and similar to the reference single foil becomes weaker and detached at the end of the downstroke and later gets annihilated as a result of interaction of the vortices shed from previous stroke.

The result of shedding of stronger trailing edge vortex, which is positioned at a higher lateral distance from the wake center, becomes evident in time-averaged wake shown in Fig. 7(a), which indicates the presence of a stronger and wider jet in the wake of the hind foil than the reference foil. Heathcote and Gursul[50] observed similar enhanced thrust from such wake signature, although produced through different means (flexible foils, in their case).

Conversely, when the phase difference between the foils is set to ($\phi = \pi/2$), the vortical structures of the foils did not have constructive interactions. The TEV-uf(1) arrives at the leading edge of the hind foil shortly after the middle of its downstroke at $t/T = 0.67$ [Fig. 5(f)]. The velocity induced by TEV-uf(1) enhances the shear-layer velocity on the hind foil, increasing the strength of LEV-dh. TEV-uf remains behind the LEV-dh until they together arrive at the trailing edge, at the end of the downstroke, where LEV-dh detaches from the trailing edge. As the upstroke begins, LEV-dh is between TEV-ud shedding from the top of the foil and TEV-uf(1) behind it, as shown in Fig. 5(g) at $t/T = 0.87$. This causes a reduction in circulation to LEV-dh as a result of vorticity annihilation. Eventually, as the result of this interaction and annihilation of the LEV-dh at $t/T = 1.07$, as shown in Fig. 5(h), smaller secondary vortices form that result in drag in the time-averaged Fig. 7(b).

Model Ar_1: The wake structures of the highest-thrust configuration of Ar_1 ($\phi = 3\pi/2$) are very similar to $Ar_{0.5}$ at $\phi = 5\pi/4$. In general, strong TEVs are present at the wake of the hind foil and the time-averaged flow field reveals a wider jet wake with higher momentum at centerline compared to the wake of the reference foil. At $t/T = 0.50$ [Fig. 8(a), Multimedia view], a single TEV-uf arrives at the leading edge of the lower surface of the hind foil, which is at that point in the middle of its upstroke. Here, the velocity induced by TEV-uf produces a shear layer at the leading-edge, forming an LEV on the bottom surface. As the foil proceeds upstroke motion, due to the proximity of TEV-uf to the surface of the hind foil, it forms a vortex pair with LEV-uh in contrast to $Ar_{0.5}$. This vortex pair remains attached to the surface of the foil and advects toward the trailing edge as seen in Fig. 8(b) (Multimedia view) ($t/T = 0.60$) and reaches the trailing edge at the end of upstroke [$t/T = 0.85$ in Fig. 8(c), Multimedia view]. Similar to $Ar_{0.5}$, due to the induced velocity of the vortex pair, LEV-uh sheds farther away from the wake centerline. However, we should note the difference that in the case of Ar_1, it is the induced LEV-uh being shed, while in the case of $Ar_{0.5}$, it is the induced TEV-uh. The start of downstroke is concurrent with the decoupling of the vortex pair. In this configuration, the decoupling is not as constructive as what seen in $Ar_{0.5}$ at $\phi = 5\pi/4$ since the vortex pair is composed of stronger vortices compared to the one in $Ar_{0.5}$. As the downstroke proceeds, the shed LEV-uf induces multiple secondary TEVs on the lower surface, and the TEV-dh merges with LEV-uf, together forming a stronger combined vortex [denoted as TEV-dh + LEV-uh in Fig. 8(d), Multimedia view]. The growth of TEV circulation shown in Fig. 6 indicates a faster TEV evolution in the case of Ar_1 than $Ar_{0.5}$.

The instantaneous vorticity field of the wake of the hind foil is similar to the one observed by Boschitsch *et al.*[32] studying in-line tandem pitching foils, where a classic reverse Bénard–von Kármán wake is observed. However, the underlying mechanism was found to be different. In their study, the induced LEV on the hind foil, which formed due to the presence of vortex arriving from the fore foil, annihilated later as it reached to the trailing edge at the end of each stroke, unlike what was observed in the current study. On the other hand, in the present study, the lower reduced frequency and higher amplitude allow the induced LEV to have enough time to reach to the trailing edge before the foil reverses direction. The higher reduced frequency in their study also has caused a narrower jet in the wake of the hind foil, producing higher thrust compared to Ar_1. Despite the differences in kinematics, however, they found a similar ideal phase differences for the spacing of $S = 3c$ ($\phi = 3\pi/2$).

The another extreme configuration of Ar_1, which produced highest drag, appeared at $\phi = 1\pi/4$. Figures 8(e)–8(h) illustrate the instantaneous vorticity field. It is shown that at $t/T = 0.50$, TEV-uf arrives at the leading edge of the hind foil when the foil has already started its downstroke. Here, TEV-uf induces an LEV of opposite sign, which subsequently detaches before the foil reaches to the middle point of its downstroke. At $t/T = 0.60$ [Fig. 8(f)], continuing the downstroke, it is seen that TEV-uf is overtaking the LEV-uh, while they advect downstream. Later, at $t/T = 0.85$, when the foil is close to the end of downstroke, the detached LEV-uh reaches at the trailing edge. At $t/T = 1.05$, as seen in Fig. 8(h), the LEV-uh is broken down in its interaction with the shear layer vortices and the TEV-uf, which has overtaken it. The resulting flow field in Fig. 8(h) looks similar to a chaotic drag producing Bénard–von Kármán vortex street. Figure 7(d)

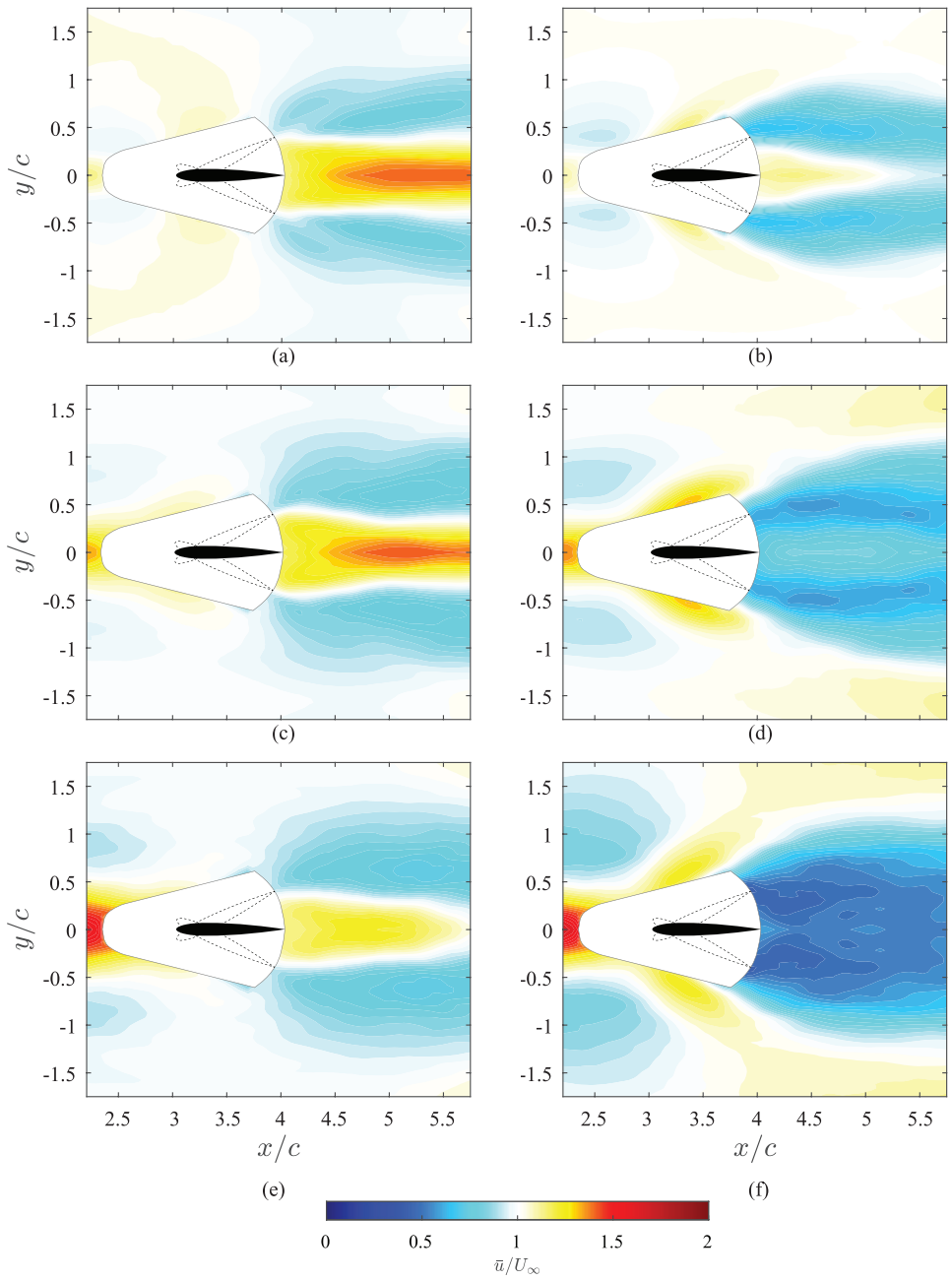

FIG. 7. Cycle-averaged streamwise velocity field of the high performance (left column) and low performance (right column) of the hind foil in tandem configurations: (a) and (b) model $Ar_{0.5}$, (c) and (d) model Ar_1, and (e) and (f) model $Ar_{1.5}$.

demonstrates the cycle-averaged velocity field of the corresponding configuration.

Model $Ar_{1.5}$: Analyzing the instantaneous flow field of the $Ar_{1.5}$, the reason for its extremely low performance becomes clear. In all configurations of $Ar_{1.5}$, a large vortex shed from the fore foil encounters the tip of the hind foil. As the result of the encounter, the vortex loses its coherence and becomes divided and decomposed into smaller vortices. The difference between the small thrust and high drag producing cases is due to the interactions of the divided vortices with the hind foil, LEV-h, and TEV-h. As further analysis of this case does little to improve our understanding of the amplitude ratio, plots of the instantaneous flow field of this model over the cycle are not presented. The instantaneous vorticity field of the hind foil at $\phi = 7\pi/4$, which is the highest thrust producing configuration of the model $Ar_{1.5}$, is

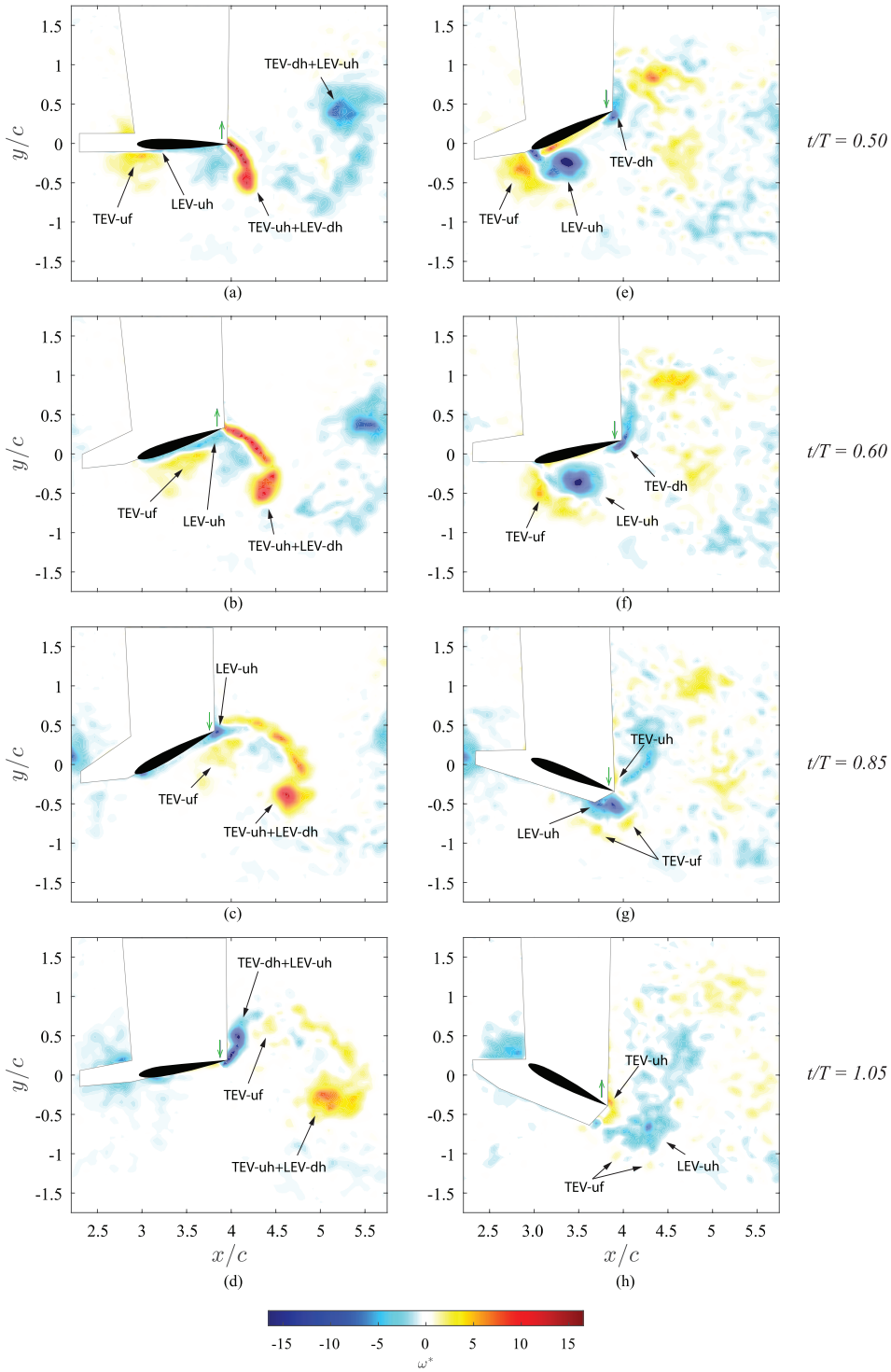

FIG. 8. Instantaneous vorticity fields of hind foil in model Ar_1 at: (a)–(d) $\phi = 3\pi/2$ corresponding to high-performance case and (e)–(h) $\phi = 1\pi/4$ corresponding to low-performance case. t/T denotes the time in the oscillation period of the fore foil. This figure illustrates the arrival of TEV-uf at the hind foil and their interactions during one oscillation cycle of the hind foil. The green arrow positioned on the trailing edge demonstrates the instantaneous direction of the foil motion. Multimedia view of Figs. 8(a)–8(d): https://doi.org/10.1063/5.0088453.3

shown in the supplementary material, Video 1. The cycle-averaged flow field of high- and low-performance configurations is presented in Figs. 7(e) and 7(f).

E. Comparison of high-thrust configurations

To synthesize the observations in Sec. III D, it has been shown that the wake of the fore foil can significantly affect the performance of the hind foil, similar to the observations of previous studies.[32–37,39] It has been demonstrated that in the high-thrust cases, a vortex pair is formed at the middle of the stroke and is shed at the end of the stroke far from the centerline. This is the underlying mechanism of thrust enhancement for both $Ar_{0.5}$ and Ar_1 configurations. The main effect of this vortex pair in constructive, thrust-enhancing configurations is an increase in TEV strength, and causing alternating TEVs to shed with a greater total wake spacing. Figure 9 summarizes the key differences of the underlying mechanisms of thrust augmentation in different amplitude ratio models at their corresponding high-performing cases. In Fig. 9(a), it is seen that in high-thrust case of $Ar_{0.5}$, the induced trailing edge vortex (TEV-dh) contributes to thrust generation. Later this vortex amalgamates with the trailing edge vortex shedding from top surface of the foil forming a stronger trailing edge vortex compared to the one shed from the isolated reference foil. Meanwhile, in the case of Ar_1 it is the induced leading edge vortex (LEV-uh) that amalgamates with the trailing edge vortices shed from the top surface, which result in formation of a stronger trailing edge vortex. TEV-uh + LEV-dh in Fig. 9(b) denotes this compound vortex shed during the previous stroke (upstroke). As seen in Fig. 9(c), in the model $Ar_{1.5}$, due to the destructive interaction of the high circulation vortex arriving from fore foil (TEV-uf) with the hind foil, the performance of the hind foil is always reduced.

Studying the differences observed in the flow fields of the high-thrust cases of $Ar_{0.5}$ and Ar_1 configurations reveals how $Ar_{0.5}$ produces thrust more effectively than Ar_1. In the high-thrust configuration of Ar_1 ($\phi = 3\pi/2$), the vortex pair that forms on the suction side of the foil is stronger than that forms on $Ar_{0.5}$ at $\phi = 5\pi/4$, which would reduce surface pressure, increasing the total lift on the surface. Although pressure on the foil surface was not determined explicitly, the instantaneous velocity field in Fig. 10 reveals a higher velocity in Ar_1, induced due to the presence of stronger vortex pair, which would result in further pressure reduction on the suction side. Given this, as thrust is the component of the instantaneous lift parallel with the free-stream, known as Knoller–Betz effect,[9] a higher thrust would be expected for Ar_1 as it generates higher lift. Despite this observation, the higher thrust achieved by $Ar_{0.5}$ at $\phi = 5\pi/4$ can be related to how effectively the wake–foil interaction in this configuration is able to tilt the lift vector in the streamwise direction. Furthermore, the weaker vortex pair on the suction side of the foil in this configuration would require less power to pitch the foil in comparison to Ar_1 at $\phi = 3\pi/2$, which augments thrust through the foil interaction with a stronger vortex pair.

Analyzing the effect of chord ratio on tandem pitching and heaving foils, Joshi and Mysa[37] observed reduced performance enhancement of the hind foil by decreasing the reduced frequency (chord size) of the fore foil, due to the reduced energy in the wake of the fore foil. In contrast to their observation, in the present study, higher performance enhancement was achieved by decreasing the Strouhal number of the fore foil (pitch amplitude) and the energy of the flow at the wake of the fore foil. Comparing Figs. 7(a), 7(c), and 7(e), it was observed that the wake of the fore foil in $Ar_{0.5}$ had lower momentum and energy, yet, at the optimum phase difference, enhances the performance of the hind more than Ar_1 and $Ar_{1.5}$ at their respective optimum phase differences. Decreasing Strouhal number also causes the wake width of the fore foil to become narrower. As shown in the Sec. III D, at the optimum phase difference, the hind foil interacts differently with the vortices of the fore foil as the wake width changes. It was observed that as the wake width of the fore foil decreased, thrust augmentation of the hind foil increased at the optimum phase difference. Therefore, the interaction between fore and hind foils cannot be predicted from the time-averaged energy or momentum of the fore-foil wake alone, but their entire time history of vortex interactions with the hind foil.

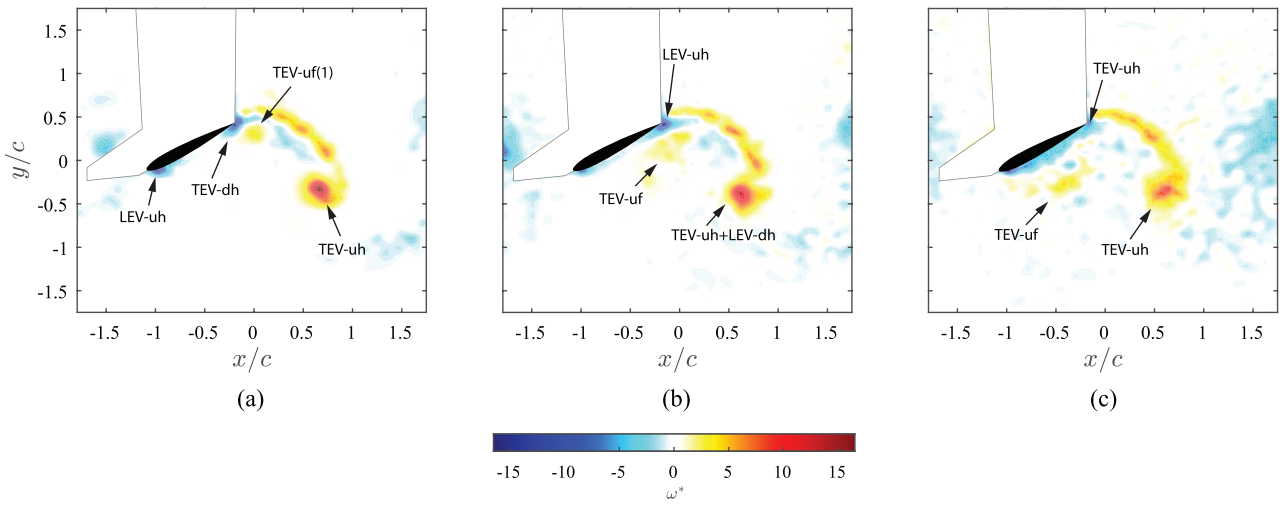

FIG. 9. Vorticity field of hind foils in highest-performing phase difference of their respective amplitude ratios: (a) $Ar_{0.5}$ at $\phi = 5\pi/4$, (b) Ar_1 at $\phi = 3\pi/2$, and (c) $Ar_{1.5}$ at $\phi = 7\pi/4$. All figures are captured at the beginning of the downstroke.

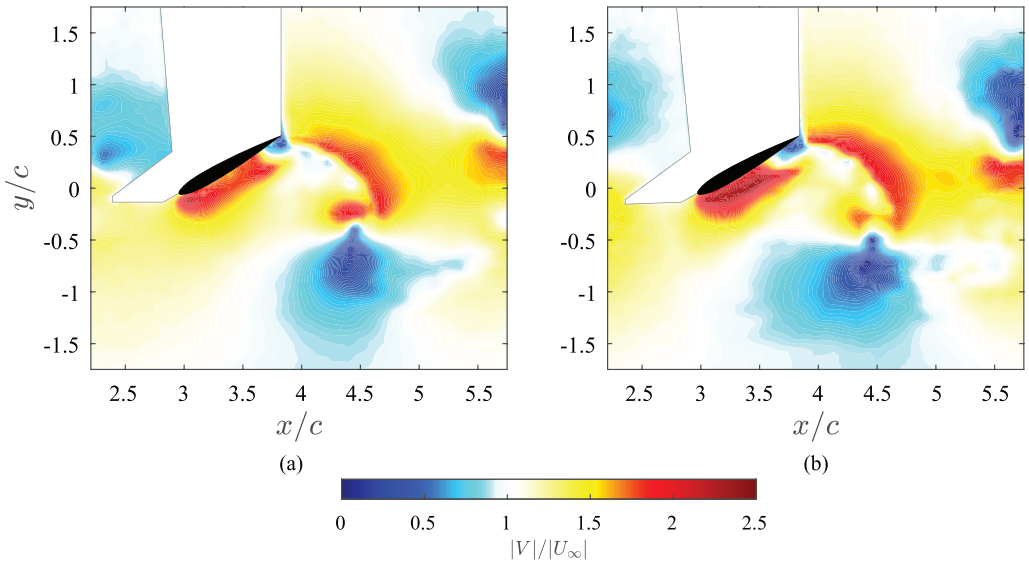

FIG. 10. Instantaneous velocity magnitude in the flow field of hind foils: (a) $Ar_{0.5}$ at $\phi = 5\pi/4$ and (b) Ar_1 at $\phi = 3\pi/2$. Both figures capture the flow field at $t/T = 0.41$ in the oscillation period of the hind foil.

F. Argument on efficiency

The propulsive efficiency of tandem foils is defined as the ratio of the power gain from the entire system to the total power given to the fluid by the tandem system, known as the Froude efficiency,

$$\eta = \frac{\bar{T}}{\bar{P}} = \frac{\bar{C}_{T,M}}{\bar{C}_{P,\mathrm{f}} + \bar{C}_{P,\mathrm{h}}}, \tag{2}$$

where η, $\bar{P}$, $\bar{C}_{T,M}$, $\bar{C}_{P,\mathrm{f}}$, and $\bar{C}_{P,\mathrm{h}}$ denote the efficiency, mean power input, mean thrust coefficient of the tandem model, and mean power coefficients of fore and hind foils, respectively. In this study, we do not have a direct measurement of the power coefficient and therefore cannot give precise values to this efficiency. However, it is possible to cautiously rank the relative efficiency of the high-thrust cases among themselves. It has been shown in the literature that the power coefficient of NACA 0012 airfoil undergoing pure pitching motion excellently scales with St^2k within $500 < Re_c < 32\,000$. Therefore, it is expected that power consumption of the fore foils, which were pitched in isolation, could be ranked based on their Strouhal number according to this scaling. Given the lower Strouhal number of the fore foil in $Ar_{0.5}$ at $\phi = 5\pi/4$, effective thrust production by the hind foil, and the highest thrust achieved among all other configurations, it could be inferred that this configuration likely had higher efficiency than Ar_1 at $\phi = 3\pi/2$. In the same manner, the high-thrust case of Ar_1 ($\phi = 3\pi/2$) likely had higher efficiency than high-thrust configuration of $Ar_{1.5}$ ($\phi = 7\pi/4$) since it produces significantly higher thrust and is expected to consume less energy in comparison. However, to confirm these speculations, explicit studies regarding the effect of amplitude ratio on efficiency are required.

In addition to the reasoning discussed above, the same observation can be inferred from the results of other studies. In the literature, it has been shown that the high thrust and high efficiency are achieved approximately concurrently in tandem in-line propulsors regardless of their motion type (pure pitching[32] or pitching and heaving).[35,41] In fact, this has been shown as one of the advantages of the tandem propulsors over isolated ones where high values of thrust are obtained at the price of lower efficiency. Joshi and Mysa[37] showed that for higher thrust producing configuration, higher efficiency has been achieved at all chord ratios of tandem foils despite an energy reduction in the wake of fore foil at smaller chord ratios. Therefore, there is a very high probability that highest thrust producing configuration of this study is nearly in phase with high efficiency. Conservatively, it can be suggested that a rear-biased locomotion could be more beneficial for a natural or a man-made vehicle employing tandem propulsion system. A future, targeted study on efficiency may confirm this suggestion.

In the paleontological context, our results indicate that plesiosaurs could likely achieve higher performance and efficiency if they had moved their hind flippers at larger amplitudes than fore flippers in cruising conditions. This suggestion is consistent with the fossil records of pliosaurs, which had more developed pelvic girdles[44,45] and are thought to be pursuit predators.[2,3] However, our findings are not consistent with the fossil records of long-necked, small-headed plesiosaurs, which show higher angular amplitude range for the fore flipper,[42,43] and a more massive development of the pectoral (shoulder) girdle when compared to hind foil.[44,45] We anticipate that although the propulsive performance was important for plesiosaurs, there were other selective pressures than efficiency for exhibiting almost identical flippers with different morphologies. However, this cannot be generalized to all plesiosaur specimens as they were diverse group of animals within their clades. Any further claims based on the results of the present study likely require a species-specific analysis, considering paleontological and biological aspects of plesiosaurs. However, the findings of this study might inform such future studies on plesiosaur locomotion.

IV. SUMMARY AND CONCLUSIONS

Inspired by the kinematics of plesiosaur flippers, PIV experiments have been conducted on two tandem pitching hydrofoils undergoing sinusoidal oscillations at high amplitudes to study the effect of

amplitude ratio on the propulsive performance. Three models of $Ar_{0.5}$, Ar_1, and $Ar_{1.5}$ studied on a range of $0 < \phi < 2\pi$ for a fixed spacing of $S = 3c$. For the first time, it has been shown that the effect of amplitude ratio on the thrust generation of hind foil is significant for spacing of $S > 1c$. Control volume analysis revealed that when the amplitude ratio was set to 0.5, highest thrust among all configurations was achieved at $\phi = 5\pi/4$, confirming our hypothesis. For this configuration, the total thrust coefficient reaches as high as 2.3 times those of an isolated foil pitching with the kinematics of the hind foil. The total thrust achieved by $Ar_{0.5}$ at $\phi = 5\pi/4$ was also 10% higher than the highest thrust producing case of amplitude ratio of Ar_1 at ($\phi = 3\pi/2$). The superiority of the total tandem system performance of $Ar_{0.5}$ configurations was evident over the entire phase difference domain. Increasing amplitude ratio to 1.5 was found to have detrimental effects on the performance of the hind foil producing negligible thrust at $\phi = 7\pi/4$ and high drag in all other configurations. It was observed that for a fixed spacing between the foils, by changing the amplitude ratio the optimum phase difference shifts.

Instantaneous vorticity field analysis showed that the highest-thrust configurations of $Ar_{0.5}$ and Ar_1 exhibit almost similar wakes where the vortices are stronger and positioned at a higher lateral distance from the centerline compared to the reference foil's wake. The time averaged of this reverse Bénard–von Kármán vortex street illustrates a high momentum jet in the wake of the hind foil. The underlying mechanism of such a wake was found to be the formation of a vortex pair at the middle and its shedding at the end of each stroke. This vortex pair consisted of TEV arriving from the fore foil and TEV (in the case of $Ar_{0.5}$) or LEV (in the case of Ar_1) induced on the suction side of the hind foil. It is observed as the wake width of the fore foil decreased with amplitude ratio, the hind foil experienced different types of wake–foil interactions to enhance thrust at the corresponding optimum phase difference. Further comparative analysis on the wake showed that the hind foil in high-thrust configuration of $Ar_{0.5}$ produces thrust more effectively than the one in Ar_1. Significantly low performance of all configurations of the $Ar_{1.5}$ model was identified to be associated with destructive encounter of hind foil with a large vortex shed from the fore foil for all phase differences studied in this model.

The results of this study suggest that hind foil in a rear-biased propulsion system benefits from enhanced performance. Although the power input to the foils was not measured explicitly in this study, using the scaling suggested by Senturk and Smits[49] for pitching NACA 0012 foils, a relative efficiency ranking between the high-thrust configurations of the tandem models was made possible. Based on the hypothetical ranking, it was argued that $Ar_{0.5}$ at $\phi = 5\pi/4$ was more efficient than the other high-thrust configurations, therefore, suggesting that a rear-biased propulsion system was more efficient. Direct measurement of power is required to confirm this suggestion. The findings of this study may inform future studies on plesiosaur swimming and efficient marine/aerial vehicle design. The present work may be extended to include effect of heave amplitude ratio, frequency ratio, cross-stream spacing between the foils, and three dimensionalities on the performance of the tandem propulsors to model more realistic biological locomotion.

SUPPLEMENTARY MATERIAL

See the supplementary material for the additional video demonstrating instantaneous vorticity field of the $Ar_{1.5}$ model at $\phi = 7\pi/4$.

ACKNOWLEDGMENTS

This work was supported by Natural Sciences and Engineering Research Council of Canada, under the Grant No. RGPIN-2018-05168.

AUTHOR DECLARATIONS

Conflict of Interest

The authors have no conflicts to disclose.

DATA AVAILABILITY

The data that support the findings of this study are available from the corresponding author upon reasonable request.

REFERENCES

[1]E. Frey and J. Riess, "Considerations concerning plesiosaur locomotion," Neues Jahrb. Geol. Palaeontol., Abh. **164**, 193–194 (1982).
[2]M. A. Taylor, "Plesiosaurs-rigging and ballasting," Nature **290**, 628–629 (1981).
[3]J. A. Massare, "Swimming capabilities of Mesozoic marine reptiles: Implications for method of predation," Paleobiology **14**, 187–205 (1988).
[4]J. M. Anderson, K. Streitlien, D. Barrett, and M. S. Triantafyllou, "Oscillating foils of high propulsive efficiency," J. Fluid Mech. **360**, 41–72 (1998).
[5]K. N. Lucas, G. V. Lauder, and E. D. Tytell, "Airfoil-like mechanics generate thrust on the anterior body of swimming fishes," Proc. Natl. Acad. Sci. **117**, 10585–10592 (2020).
[6]X. Wu, X. Zhang, X. Tian, X. Li, and W. Lu, "A review on fluid dynamics of flapping foils," Ocean Eng. **195**, 106712 (2020).
[7]R. Knoller and O. Verein, *Die Gesetze des Luftwiderstandes* (Verlag des Osterreichischer Flugtechnischen Vereines, 1909).
[8]A. Betz, "Ein beitrag zur erklaerung segelfluges," Z. Flugtech. Motorluftschiffahrt **3**, 269–272 (1922).
[9]R. Katzmayr, "Effect of periodic changes of angle of attack on behavior of airfoils," Technical Report No. NACA-TM-147, 1922.
[10]Y. S. Baik, L. P. Bernal, K. Granlund, and M. V. Ol, "Unsteady force generation and vortex dynamics of pitching and plunging aerofoils," J. Fluid Mech. **709**, 37–68 (2012).
[11]M. M. Koochesfahani, "Vortical patterns in the wake of an oscillating airfoil," AIAA J. **27**, 1200–1205 (1989).
[12]R. Godoy-Diana, J.-L. Aider, and J. E. Wesfreid, "Transitions in the wake of a flapping foil," Phys. Rev. E **77**, 016308 (2008).
[13]D. G. Bohl and M. M. Koochesfahani, "MTV measurements of the vortical field in the wake of an airfoil oscillating at high reduced frequency," J. Fluid Mech. **620**, 63–88 (2009).
[14]M. Wolfgang, J. Anderson, M. Grosenbaugh, D. Yue, and M. Triantafyllou, "Near-body flow dynamics in swimming fish," J. Exp. Biol. **202**, 2303–2327 (1999).
[15]E. G. Drucker and G. V. Lauder, "Locomotor function of the dorsal fin in teleost fishes: Experimental analysis of wake forces in sunfish," J. Exp. Biol. **204**, 2943–2958 (2001).
[16]M. Triantafyllou, G. Triantafyllou, and R. Gopalkrishnan, "Wake mechanics for thrust generation in oscillating foils," Phys. Fluids A **3**, 2835–2837 (1991).
[17]G. K. Taylor, R. L. Nudds, and A. L. Thomas, "Flying and swimming animals cruise at a Strouhal number tuned for high power efficiency," Nature **425**, 707–711 (2003).
[18]D. A. Read, F. Hover, and M. Triantafyllou, "Forces on oscillating foils for propulsion and maneuvering," J. Fluids Struct. **17**, 163–183 (2003).
[19]K. Jones, C. Dohring, and M. Platzer, "Experimental and computational investigation of the Knoller–Betz effect," AIAA J. **36**, 1240–1246 (1998).
[20]W. Birnbaum, "Das ebene problem des schlagenden flügels," ZAMM-J. Appl. Math. Mech./Z. Angew. Math. Mech. **4**, 277–292 (1924).
[21]G. Liu, Y. Ren, H. Dong, O. Akanyeti, J. C. Liao, and G. V. Lauder, "Computational analysis of vortex dynamics and performance enhancement due to body–fin and fin–fin interactions in fish-like locomotion," J. Fluid Mech. **829**, 65–88 (2017).

[22]E. Salami, T. A. Ward, E. Montazer, and N. N. N. Ghazali, "A review of aerodynamic studies on dragonfly flight," Proc. Inst. Mech. Eng., Part C **233**, 6519–6537 (2019).
[23]I. Akhtar, R. Mittal, G. V. Lauder, and E. Drucker, "Hydrodynamics of a biologically inspired tandem flapping foil configuration," Theor. Comput. Fluid Dyn. **21**, 155–170 (2007).
[24]D. Rival, G. Hass, and C. Tropea, "Recovery of energy from leading-and trailing-edge vortices in tandem-airfoil configurations," J. Aircr. **48**, 203–211 (2011).
[25]T. M. Broering, Y. Lian, and W. Henshaw, "Numerical investigation of energy extraction in a tandem flapping wing configuration," AIAA J. **50**, 2295–2307 (2012).
[26]D. Weihs, "Hydromechanics of fish schooling," Nature **241**, 290–291 (1973).
[27]D. Weihs and T. Y. T. Wu, *Swimming and Flying in Nature* (Springer, 1975).
[28]H. Yu, X.-Y. Lu, and H. Huang, "Collective locomotion of two uncoordinated undulatory self-propelled foils," Phys. Fluids **33**, 011904 (2021).
[29]A. Gungor, M. S. U. Khalid, and A. Hemmati, "How does switching synchronization of pitching parallel foils from out-of-phase to in-phase change their wake dynamics?," Phys. Fluids **33**, 081901 (2021).
[30]P. B. Lissaman and C. A. Shollenberger, "Formation flight of birds," Science **168**, 1003–1005 (1970).
[31]D. Hummel, "Aerodynamic aspects of formation flight in birds," J. Theor. Biol. **104**, 321–347 (1983).
[32]B. M. Boschitsch, P. A. Dewey, and A. J. Smits, "Propulsive performance of unsteady tandem hydrofoils in an in-line configuration," Phys. Fluids **26**, 051901 (2014).
[33]M. Kurt and K. W. Moored, "Flow interactions of two-and three-dimensional networked bio-inspired control elements in an in-line arrangement," Bioinspiration Biomimetics **13**, 045002 (2018).
[34]T. M. Broering and Y.-S. Lian, "The effect of phase angle and wing spacing on tandem flapping wings," Acta Mech. Sin. **28**, 1557–1571 (2012).
[35]L. Muscutt, G. Weymouth, and B. Ganapathisubramani, "Performance augmentation mechanism of in-line tandem flapping foils," J. Fluid Mech. **827**, 484–505 (2017).
[36]G. Xu, W. Duan, and W. Xu, "The propulsion of two flapping foils with tandem configuration and vortex interactions," Phys. Fluids **29**, 097102 (2017).
[37]V. Joshi and R. C. Mysa, "Mechanism of wake-induced flow dynamics in tandem flapping foils: Effect of the chord and gap ratios on propulsion," Phys. Fluids **33**, 087104 (2021).
[38]L. Cong, B. Teng, and L. Cheng, "Hydrodynamic behavior of two-dimensional tandem-arranged flapping flexible foils in uniform flow," Phys. Fluids **32**, 021903 (2020).
[39]M. Kurt, A. Mivehchi, and K. Moored, "High-efficiency can be achieved for non-uniformly flexible pitching hydrofoils via tailored collective interactions," Fluids **6**, 233 (2021).
[40]S. Tarsitano and J. Riess, "Plesiosaur locomotion-underwater flight versus rowing," Neues Jahbr. Geol. Palaeontol., Abh. **164**, 188–192 (1982).
[41]L. E. Muscutt, G. Dyke, G. D. Weymouth, D. Naish, C. Palmer, and B. Ganapathisubramani, "The four-flipper swimming method of plesiosaurs enabled efficient and effective locomotion," Proc. R. Soc. B **284**, 20170951 (2017).
[42]S. Liu, A. S. Smith, Y. Gu, J. Tan, C. K. Liu, and G. Turk, "Computer simulations imply forelimb-dominated underwater flight in plesiosaurs," PLoS Comput. Biol. **11**, e1004605 (2015).
[43]K. Carpenter, F. Sanders, B. Reed, J. Reed, and P. Larson, "Plesiosaur swimming as interpreted from skeletal analysis and experimental results," Trans. Kansas Acad. Sci. **113**, 1–34 (2010).
[44]F. R. O'Keefe, "The evolution of plesiosaur and pliosaur morphotypes in the plesiosauria (Reptilia: Sauropterygia)," Paleobiology **28**, 101–112 (2002).
[45]F. R. O'Keefe and M. T. Carrano, "Correlated trends in the evolution of the plesiosaur locomotor system," Paleobiology **31**, 656–675 (2005).
[46]T. L. Hilderman, "Measurement, modelling, and stochastic simulation of concentration fluctuations in a shear flow," Ph.D. thesis (Department of Mechanical Engineering, University of Alberta, 2004).
[47]L. Muscutt, "The hydrodynamics of plesiosaurs," Ph.D. thesis (University of Southampton, 2017).
[48]M. Raffel, C. E. Willert, and J. Kompenhans, *Particle Image Velocimetry: A Practical Guide*, 3rd ed. (Springer International Publishing AG, Cham, Switzerland, 2018).
[49]U. Senturk and A. J. Smits, "Reynolds number scaling of the propulsive performance of a pitching airfoil," AIAA J. **57**, 2663–2669 (2019).
[50]S. Heathcote and I. Gursul, "Flexible flapping airfoil propulsion at low Reynolds numbers," AIAA J. **45**, 1066–1079 (2007).